Retention of δ–ferrite in Aluminium–Alloyed TRIP–assisted steels

Young Joo Choi[1], Dong–Woo Suh[1] and H. K. D. H. Bhadeshia[1,2]

[1]Graduate Institute of Ferrous Technology (GIFT)
Pohang University of Science and Technology (POSTECH)
Pohang 790-784, Republic of Korea

[2]University of Cambridge
Materials Science and Metallurgy, Cambridge CB2 3QZ, U.K.

Abstract

There have been significant difficulties in the theory for the optimisation of δ–TRIP steel since the original concept was invented. In particular, the prediction of phase fractions has been notoriously unreliable using standard thermodynamic methods. New thermodynamic databases have become available and seem to explain both published and new experiments conducted to probe the data. Solidification experiments are reported in order to test the non–equilibrium retention of excess δ–ferrite in the microstructure observed at ambient temperature. These provided valuable information for comparison against kinetic simulations which prove that the excess ferrite cannot be attributed to growth phenomena. Instead, evidence is offered to show that it is the difficulty in nucleating austenite which prevents the thermodynamically required transformation of δ–ferrite.

1. Introduction

Popular steels which exploit transformation–induced plasticity have a microstructure which is predominantly allotriomorphic ferrite, with the remainder consisting of a mixture of bainitic ferrite and retained austenite (DeCooman, 2004; Jacques, 2004; Matsumura et al., 1987a,b). The allotriomorphic ferrite is generated either by transformation from austenite, or by intercritical annealing (Bhadeshia, 2001). There may be an advantage in replacing such ferrite with stable δ–ferrite which is retained from the solidification process (Chatterjee et al., 2007; Yi et al., 2011a). This is because the steel cannot ever be made fully austenitic. This means that it is not possible during resistance spot–welding to create a fully martensitic heat–affected zone, which because of the high carbon concentration, embrittles the joint. The new class of steel which relies on the permanent presence of δ–ferrite is

known by the name δ–TRIP steel and seems to show extraordinary combinations of mechanical properties (Yi et al., 2011a).

It is known in this context, that alloying with aluminium makes the δ–phase more thermodynamically stable. Recent attempts at designing low–alloy steels in which the microstructure retains a large fraction of δ–ferrite have come up against difficulties in which the quantity of δ–ferrite is sometimes grossly overestimated using standard phase diagram calculations (Yi et al., 2010), thus necessitating the empirical study of a series of seven alloys with varying aluminium contents (Jung et al., 2012; Yi et al., 2011b). An attempt was made to explain the discrepancies using kinetic simulations and microanalytical data, resulting in a conclusion that the problem arises due to the inadequate partitioning of substitutional solute as austenite grows from δ–ferrite.

A further possibility is that the thermodynamic database on which the original phase diagram and kinetic calculations were conducted is imprecise when it comes to the estimation of aluminium effects. Indeed, a more recent version of the database (TCFE 6.2) includes a reassessment of the Fe–Al–C system and of the relative stabilities of the austenite and ferrite phases (Bratberg, 2011). Experiments to verify these propositions are also reported here.

The purpose of the present work was to study the retention of δ–ferrite in detail using the TCFE6 database in association with kinetic simulations and controlled–solidification experiments in order to establish whether the alloy design procedures can be improved for this promising variety of δ–TRIP steel.

2. Experimental and Simulation procedures

The chemical compositions of alloys used in this work are listed in Table 1. These were fabricated by vacuum induction melting and cast as 25 kg ingots. Part of each ingot was austenitised at 1200 °C for 1 h followed by hot rolling to 4.5 mm in thickness with the finishing–rolling temperature above 950 °C. Cylindrical specimens 298 mm long and 4 mm diameter were machined for the controlled solidification experiments. The solidification experiment was performed using the apparatus shown in Fig. 1 (Lee, 2008). The specimen was melted in a 298 mm long alumina tube with outer and inner diameters of 10 and 5.5 mm respectively. The tube was then withdrawn from the induction furnace into a water–cooled device section at 3 and 300 mm min^{-1}, corresponding to cooling rates of 0.4 and 8.1 °C s^{-1}, respectively. Interrupted quenching was conducted to freeze the microstructure. In order to assess the temperature at which the sample is quenched, a thermocouple was inserted into the hot zone without the presence of a sample, and withdrawn at the same rate as the sample. The temperature was found not to be constant throughout the hot zone so in what follows, the quench temperature is stated as a range, since rather than a precise value because of this instrumental limitations.

For microstructural characterisation, the specimen was cut along the longitudinal axis and the vertical section observed. Optical microscopy was on samples etched with 2% nital or Oberhoffer's solution (0.5 g $SnCl_2$, 1 g $CuCl_2$, 30 g $FeCl_3$, 500 ml distilled water, 500 ml ethanol, 50 ml HCl). The volume fraction of ferrite was measured using point counting on the optical micrographs.

Solidification was simulated by considering effectively the one–dimensional solidification of a bar sample, using DICTRA software (Andersson and Ågren, 1992) and mobility database MOB2 (Anonymous, 2008a) with the cell size set to be consistent with the observed microstructure (Zhang et al., 2012), i.e., 60 μm and 21 μm for 0.4 and 8.1 $^{\circ}C\,s^{-1}$ cooling rates, respectively. Equilibrium phase fractions were evaluated with Thermocalc software (Sundman et al., 1985) using database TCFE6 (Anonymous, 2008b).

Table 1. Chemical compositions (wt%) of alloys

Sample	C	Si	Mn	Al	Cu	Reference
Alloy 1	0.30	0.20	0.52	3.5		Present work
Alloy 3	0.31	0.21	0.51	5.6		Present work
Alloy 5	0.40	0.19	0.51	3.5		Present work
Alloy 7	0.39	0.19	0.50	5.6		Present work
Alloy A	0.36	0.26	2.02	2.1	0.49	(Yi et al., 2010)
Alloy B	0.37	0.23	1.99	2.59	0.49	(Yi et al., 2010)

3. Results and Discussion

(a) Validity of Thermodynamic Data

A quick calculation using both the TCFE4 and TCFE6 databases shows dramatic differences for the type of alloys of interest to us in the context of the δ–TRIP steels (Fig. 2a,b). A simple experiment in which alloy 3 was held at 1300°C for 24 h and then quenched, revealed a quantity of δ–ferrite which is more consistent with calculations based on the TCFE6 database. It is apparent from Fig. 2d that the thermodynamic database correctly predicts the fractions in all four alloys following prolonged heat treatment at 1300°C.

The difficulties encountered in previous work on Alloys A and B (Table 1), where the amount of δ–ferrite was observed to be absent or much smaller than equilibrium calculations using the TCFE1.2 database, are also resolved as shown in Fig. 3. It is seen that the alloys can in fact become fully austenitic over a large temperature range because of the much greater manganese and copper

4

concentrations, and much lower aluminium concentrations. The former two solutes stabilise austenite whereas the aluminium promotes ferrite.

(b) As–cast microstructures

Fig. 4 shows the clear retention of δ–ferrite dendrites in the as–cast microstructures; alloys 1 and 3 contain more ferrite in the cast condition than alloys 5 and 7, a trend that is consistent with the maximum fractions of ferrite expected at equilibrium with austenite (Fig. 5). It is noteworthy that alloy 5 during cooling passes through a temperature range where it can in principle become fully austenitic, but δ–ferrite is nevertheless retained. It is apparent that there is an excess of dendritic ferrite in the as–cast alloys, possibly because of the actual cooling rate during solidification is too fast to achieve equilibrium.

(c) Controlled solidification and kinetic simulation

Fig. 6 shows the microstructures of specimens subjected to the controlled–solidification experiment at $8.1\,^{\circ}\mathrm{C\,s}^{-1}$ and then quenched from between 1130–1270 $^{\circ}$C corresponding roughly to the range in which the fraction of ferrite under equilibrium conditions becomes minimum before increasing on cooling. The ferrite fractions in the quenched microstructures are about 0.5 and similar in all four alloys; actual fractions are indicated on the micrographs. The skeletal form of the δ–dendrites indicates for alloys 1 and 5, that the transformation of the δ–ferrite is incomplete, contrary to what might be expected from the equilibrium phase diagrams shown in Fig. 5. The microstructure of alloy 5 solidified at the much slower rate of $0.4\,^{\circ}\mathrm{C\,s}^{-1}$ is shown in Fig. 7. It is clear that the cooling rate has a remarkable effect on the presence of δ–ferrite. The slow cooling rate has clearly consumed much more of the δ–ferrite, as indicated both by the smaller fraction and larger spacing between the remnants of the ferrite. Kinetic phenomena are clearly hindering the transformation of δ–ferrite for the cooling rates studied.

Given that the formation of austenite involves a peritectic reaction, it is tempting to attribute the excess δ ferrite to the fact that such reactions involve the combined action of three phases $(L + \delta \rightarrow \gamma)$ in which the reactants can become isolated by the product. Such isolation then requires diffusion through the thickening product and hence leads to a reduction in reaction rate except at the slowest of cooling rates. To study whether this is the answer, we conducted one–dimensional solidification simulations using DICTRA (Anonymous, 2008a), which deals with multicomponent diffusional transformations, but only with the growth part of the process; there is no nucleation in the simulation, the phases are allowed to exist from time zero. Thus, a layer of austenite forms between the liquid and δ ferrite as might happen with a peritectic reaction. The one–dimensional nature of the simulation, with flat interfaces between the phases should yield slower rates of solidification than when cylindrical or spherical shapes are considered. However, as shown in Fig. 8, the quantity of δ–ferrite keeps pace with the equilibrium phase diagram leading to the inevitable conclusion that the observed excess volume fractions cannot be explained in terms of the growth of phases or the nature

of the peritectic reaction. It also remains to explain, as illustrated in Fig. 8, why the discrepancy between the observed (V_δ^{obs}) and equilibrium fraction (V_δ^{eq}) varies dramatically for the different alloys, being greatest for Alloy 5 and least for Alloy 3.

The temperature range over which austenite forms is very narrow, as shown in the expanded phase diagrams presented in Fig. 9a, and varies over only a few degrees centigrade. Nevertheless, it has been demonstrated that growth at the temperatures involved is sufficiently rapid to maintain phase fractions close to expectations from equilibrium. The remaining, and it seems, likely possibility for explaining the retention of excess δ is that it is difficult for austenite to nucleate within this very narrow temperature interval. An interesting experiment has been reported which demonstrated with clarity, the difficulty of nucleating austenite in liquid steel (Bhadeshia et al., 1991). In this, a laser was traversed across dissimilar steels placed in edge contact, one being an austenitic and the other a ferritic stainless steel; the laser was sufficiently powerful to melt the substrate and create liquid. When the direction of traverse was from the austenitic to the ferritic steel, the austenite dendrites simply grew across the junction and forced the ferritic stainless steel to solidify as austenite. However, a traverse in the reverse direction simply stopped the δ–ferrite dendrites stopped abruptly on reaching the austenitic alloy. The experiment proved that by completely removing the need to nucleate austenite, it was possible to convert liquid steel which would normally solidify as δ–ferrite, into metastable austenite. The barrier to the nucleation of austenite is otherwise large.

We believe, that having eliminated the role of growth, the retention of excess δ–ferrite must be attributed to the difficulty in nucleating austenite over the narrow equilibrium–temperature range over which the austenite needs to exist. And the discrepancy in the volume fraction of δ–ferrite (i.e, $V_\delta^{obs} - V_\delta^{eq}$) correlates directly with the amount of $V_{\delta\to\gamma}^{eq}$ of δ–ferrite that must transform into austenite over that narrow temperature range, as shown in Fig. 9b. Obviously, the larger the value of $V_{\delta\to\gamma}^{eq}$, the greater would be the need for austenite nuclei. Notice that such a correlation cannot be expected if the process is growth limited via the peritectic mechanism, since all interfaces would be involved in the thickening of austenite layers irrespective of the amount of δ/L interface originally available.

4. Conclusions

A number of issues have been resolved which should assist in the future design of the so–called δ–TRIP steels and indeed in the generic problem of δ–ferrite retention:

1. It has been demonstrated, both by conducting elevated temperature equilibrium heat–treatment experiments, and by rationalising previous data (Yi et al., 2010), that the recent thermodynamic databases are able to

correctly represent phase stabilities, specifically in the context of the δ–TRIP steels.

2. It has been shown by simulation of new solidification experiments, that the retention of excess $\dot{\delta}$–ferrite is not attributable in a range of alloys studied, to the growth process during the peritectic reaction. The growth kinetics are sufficiently rapid for the phase fractions to essentially keep up with equilibrium fractions as the steel cools.

3. The retention of excess δ–ferrite has a strong dependence on the nature of the alloy, but this correlates strongly with the equilibrium quantity of δ–ferrite that is required to transform into austenite over a narrow temperature range. This observation together with evidence from previous work suggests that it is the difficulty in nucleating austenite that is responsible for the retention of excess ferrite.

References

Andersson, J. O., Ågren, J. A., 1992. Models for numerical treatment of multicomponent diffusion in simple phases. Journal of Applied Physics 72, 1350–1355.

Anonymous, 2008a. DICTRA user's guide (version 26). Tech. rep., Thermo–Calc software AB, Stockholm, Sweden.

Anonymous, 2008b. Thermo-Calc user's guide (version S). Tech. rep., Thermo–Calc software AB, Stockholm, Sweden.

Bhadeshia, H. K. D. H., 2001. Bainite in Steels, 2nd edition. Institute of Materials, London.

Bhadeshia, H. K. D. H., David, S. A., Vitek, J. M., 1991. Solidification sequences in stainless steel dissimilar alloy welds. Materials Science and Technology 7, 50–61.

Bratberg, J., 2011. TCFE6–TCS Steels/Fe–Alloys Database, Version 6.2. Tech. rep., Thermo–Calc software AB, Stockholm, Sweden.

Chatterjee, S., Murugananth, M., Bhadeshia, H. K. D. H., 2007. δ–TRIP steel. Materials Science and Technology 23, 819–827.

DeCooman, B., 2004. Structure–properties relationship in TRIP steels containing carbide-free bainite. Current Opinion in Solid State and Materials Science 8, 285–303.

Jacques, P. J., 2004. Transformation-induced plasticity for high strength formable steels. Current Opinion in Solid State and Materials Science 8, 259–265.

Jung, G. S., Lee, K. Y., Lee, J. B., Bhadeshia, H. K. D. H., Suh, D.-W., 2012. Spot weldability of TRIP assisted steels with high carbon and aluminium contents. Science and Technology of Welding and Joining 17, 92–98.

Lee, S. B., 2008. Change in morphology of MnS inclusions in steel duirng unidirectional solidification. Ph.D. thesis, Pohang University of Science and Technology, Pohang, Republic of Korea.

Matsumura, O., Sakuma, Y., Takechi, H., 1987a. Enhancement of elongation by retained austenite in intercritical annealed 0.4C-1.5Si-0.8Mn steel. Transactions of the Iron and Steel Institute of Japan 27, 570–579.

Matsumura, O., Sakuma, Y., Takechi, H., 1987b. TRIP and its kinetic aspects in austempered 0.4C-1.5Si-0.8Mn steel. Scripta Metallurgica 27, 1301–1306.

Sundman, B., Jansson, B., Andersson, J. O., 1985. The Thermo–Calc databank system. CALPHAD 9, 153–190.

Yi, H. L., Ghosh, S. K., Liu, W. J., Lee, K. Y., Bhadeshia, H. K. D. H., 2010. Nonequilibrium solidification and ferrite in δ–TRIP steel. Materials Science and Technology 26 (817–823).

Yi, H. L., Lee, K. Y., Bhadeshia, H. K. D. H., 2011a. Extraordinary ductility in Al–bearing δ–TRIP steel. Proceedings of the Royal Society A 467, 234–243.

Yi, H. L., Lee, K. Y., Bhadeshia, H. K. D. H., 2011b. Stabilisation of ferrite in hot-rolled in δ–TRIP steel. Materials Science and Technology 27, 525–529.

Zhang, G., Wei, R., Enomoto, M., Suh, D. W., 2012. Growth kinetics of proeutectoid ferrite in Fe-0.1C-1.5Mn-1Si quaternary and Fe-0.1C-1.5Mn-1Si-0.2Al quinary alloys. Metallurgical & Materials Transactions A 43, DOI: 10.1007/s11661–011–1000–9.
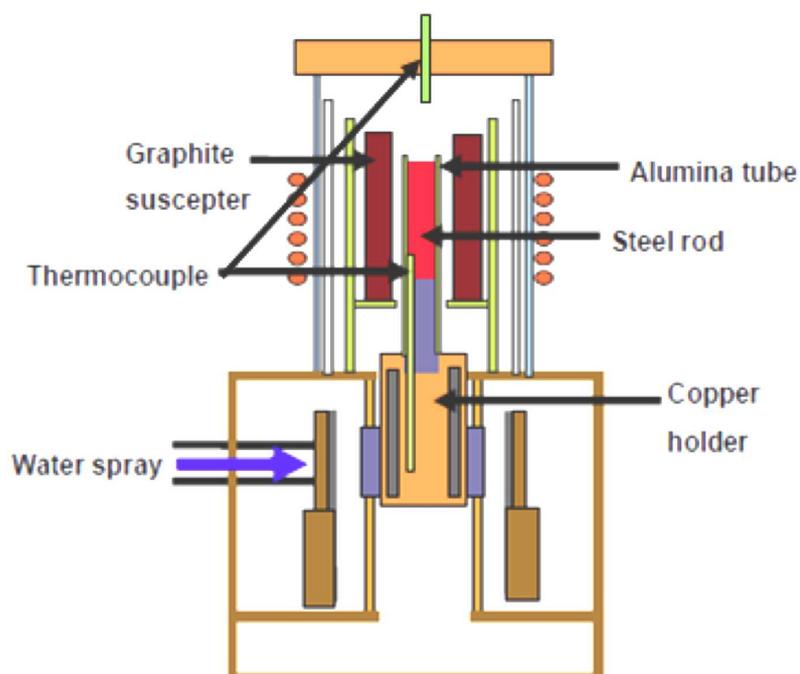
Figure 1. Controlled–solidification apparatus.
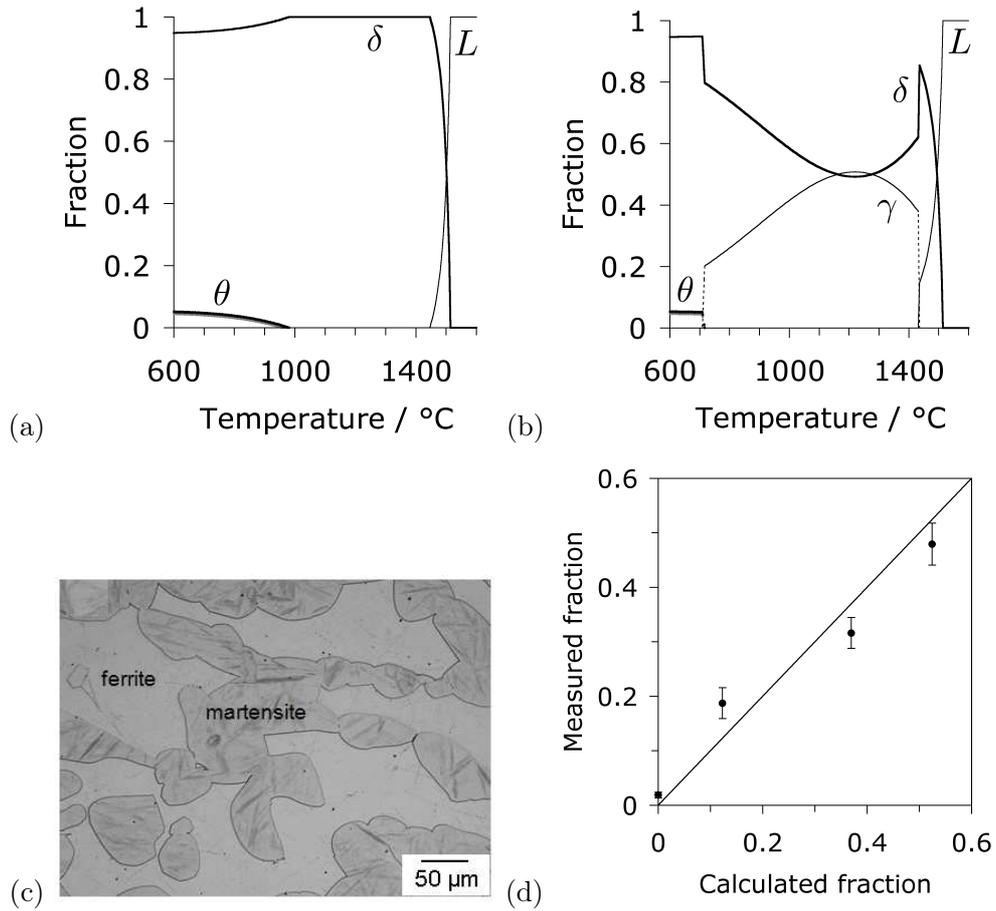
Figure 2. Equilibrium phase fractions for Fe–0.3C–0.5Mn-0.2Si-5.6Al wt% steel, The symbols δ, γ, L and θ stand for ferrite, austenite, liquid and cementite respectively. (a) Calculated with TCFE4, (b) calculated with TCFE6 thermodynamic database. (c) Micrograph of alloy 3 held at 1300 °C for 24 h prior to quenching to room temperature. (d) As for (c) but data for all alloys, with the fraction increasing in the order alloy 5, 1, 7, 3.
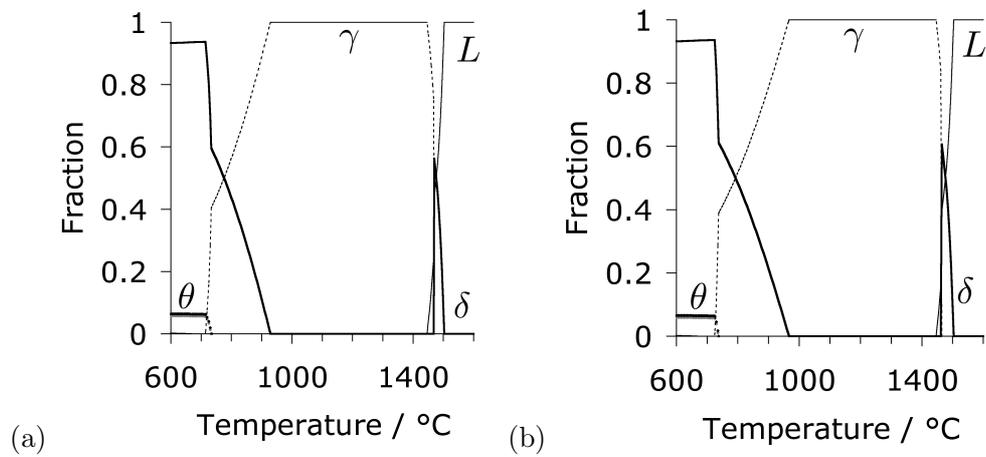
Figure 3. Equilibrium phase fractions for Alloys A and B (Table 1) calculated with TCFE6 thermodynamic database.
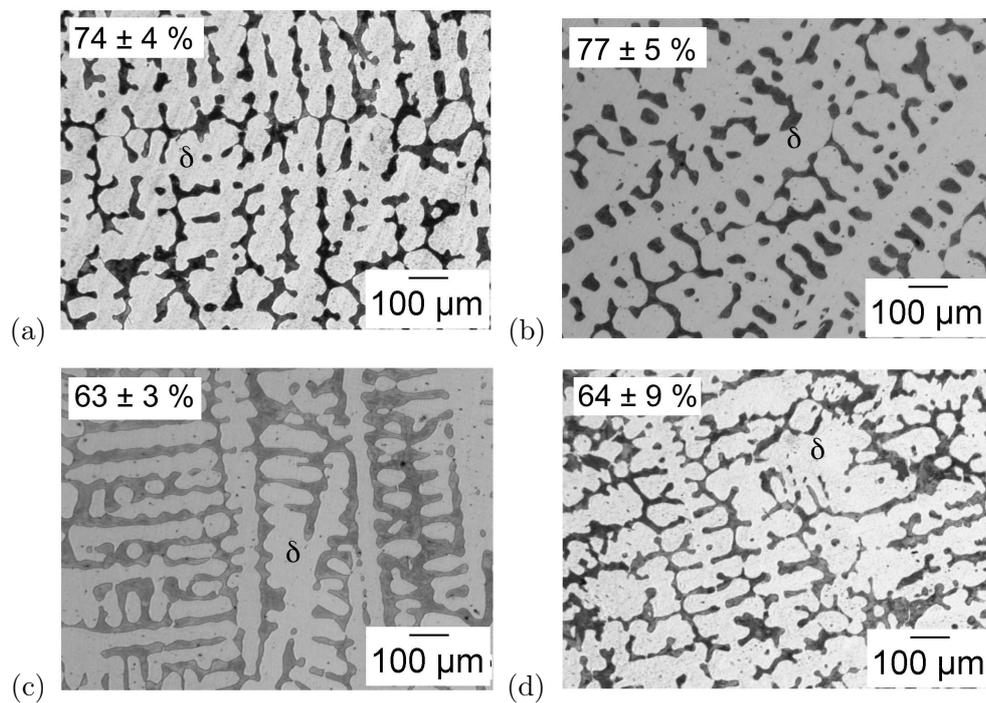
Figure 4. As–cast alloys. (a) Alloy 1, (b) alloy 3, (c) alloy 5 and (d) alloy 7.
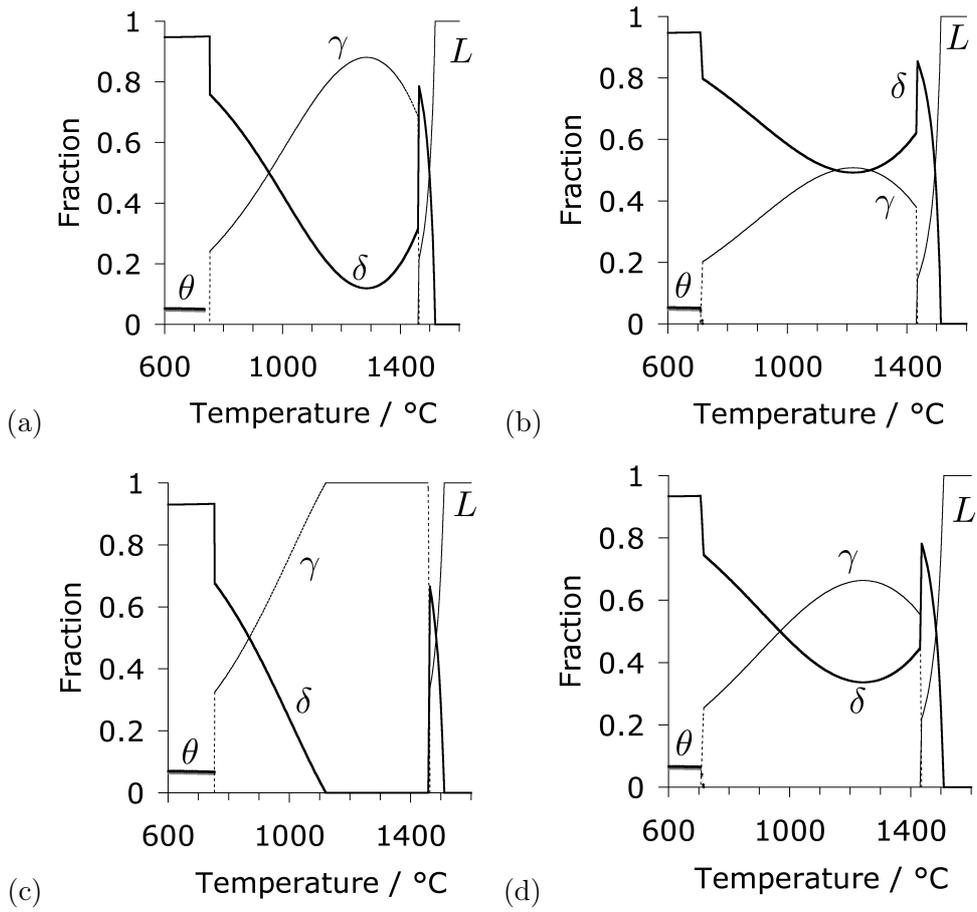
Figure 5. Equilibrium phase fractions. (a) Alloy 1, (b) alloy 3, (c) alloy 5 and (d) alloy 7.
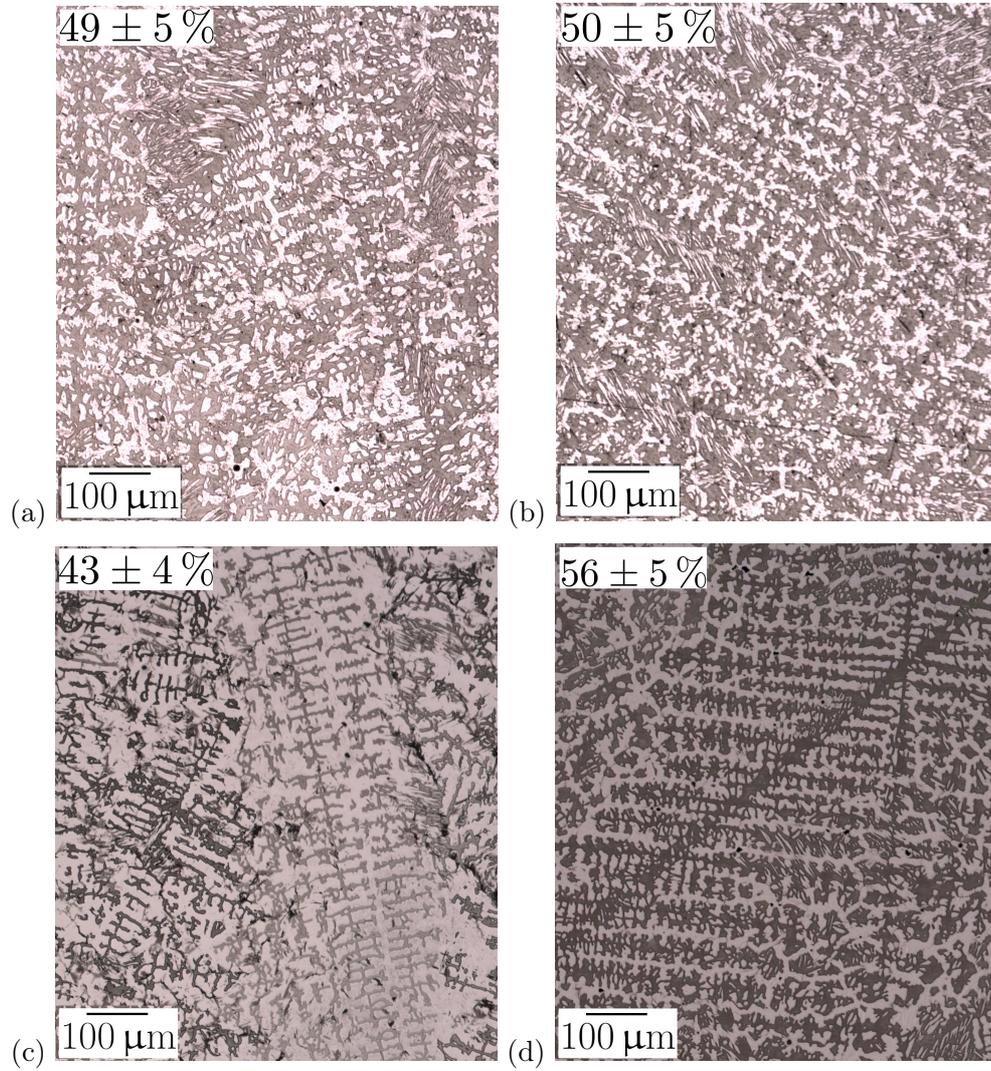
Figure 6. Micrographs of alloys solidified at $8.1\,^{\circ}\mathrm{C\,s^{-1}}$ and quenched from 1130–1270 °C. (a) Alloy 1, (b) alloy 3, (c) alloy 5 and (d) alloy 7. The numbers at the top of each represent percentage ferrite with uncertainty quoted at $\pm 1\sigma$.
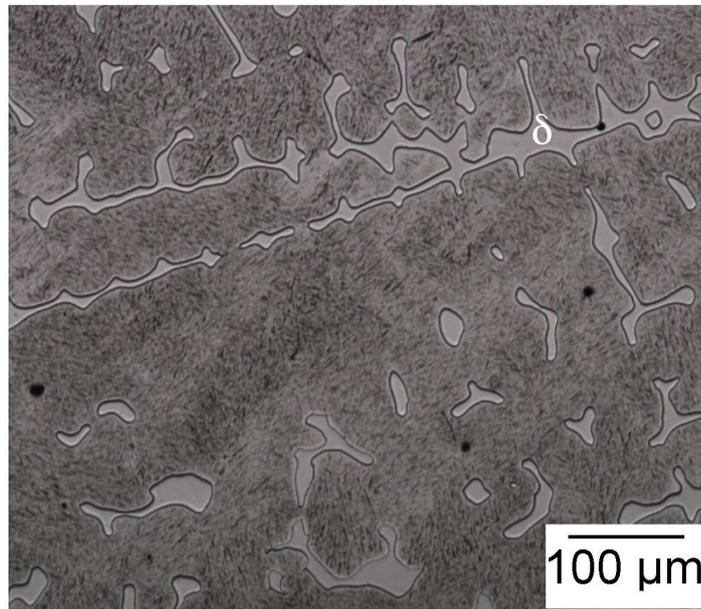
Figure 7. Micrograph of alloy 5 solidified at $0.4\,^\circ\mathrm{C}\,\mathrm{s}^{-1}$ and quenched from 1210–1260 $^\circ$C.
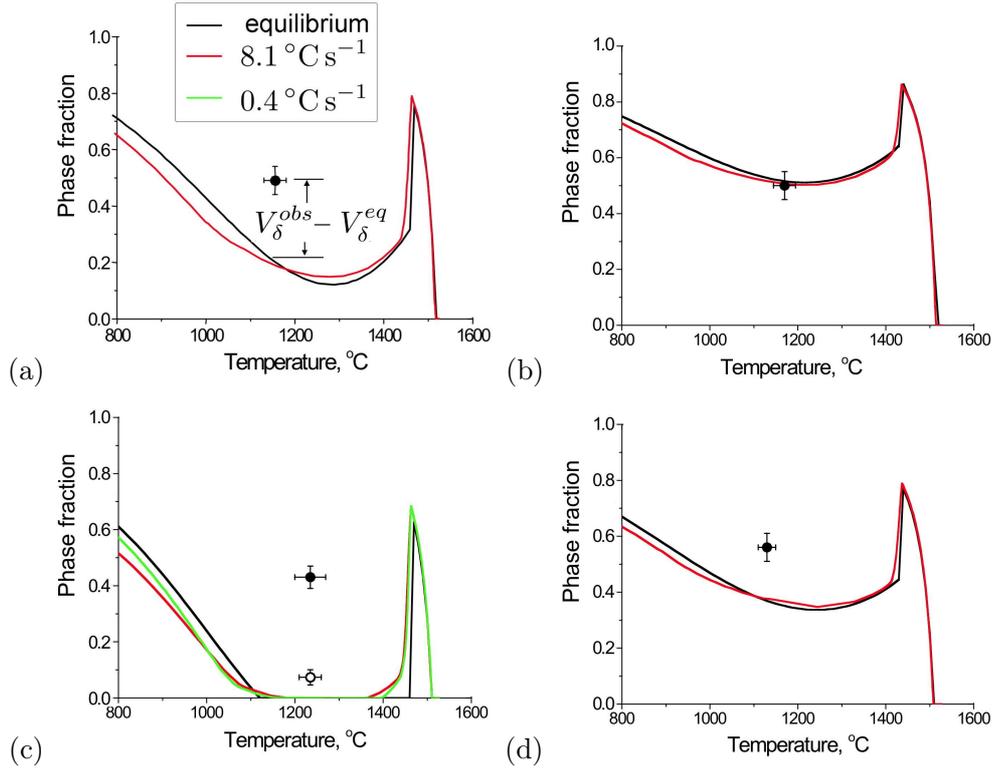
Figure 8. Ferrite fraction from equilibrium calculation and kinetic simulation. Symbols represent the measured ferrite fraction at a cooling rate of $8.1\,^{\circ}\mathrm{C}\,\mathrm{s}^{-1}$ (solid) and $0.4\,^{\circ}\mathrm{C}\,\mathrm{s}^{-1}$ (open), respectively. (a) alloy 1, (b) alloy 3, (c) alloy 5 and (d) alloy 7. The numbers at the top of each represent percentage ferrite with uncertainty quoted at $\pm 1\sigma$. The horizontal bars on the experimental data represent in each case the uncertainty in the quench temperature.

(a)

(b)
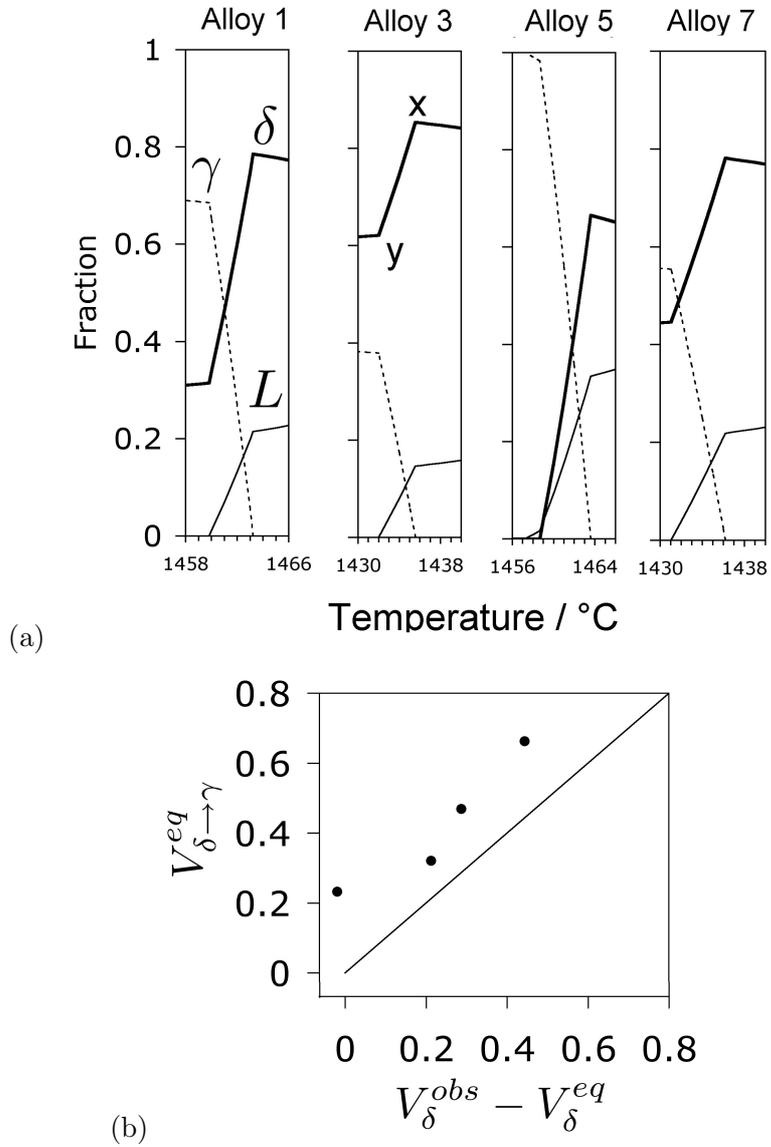
Figure 9. (a) Equilibrium phase diagrams focusing on the reactions that lead to austenite formation. The vertical distance beween x and y is defined as $V_{\delta \to \gamma}^{eq}$, the amount of d that must convert to γ over a temperature range which is only about 5°C. (b) $V_{\delta \to \gamma}^{eq}$ as a function of the amount of δ observed in excess of that expected from equilibrium at the quenching temperature.